Available online at www.sciencedirect.com
ScienceDirect
Catalysis Today 118 (2006) 410–415
CATALYSIS TODAY
www.elsevier.com/locate/cattod

Formation of the nanocrystalline mesoporous niobium-silicon oxynitride

Izabela Nowak *, Maria Ziolek

Adam Mickiewicz University, Faculty of Chemistry, Grunwaldzka 6, PL-60-780 Poznan, Poland

Available online 1 September 2006

Abstract

A new method for the preparation of crystalline mesoporous niobium-silicon oxynitride (NbSiON) by the straightforward technique is described. The characterization has been performed by various techniques showing that the material has: (i) the specific surface area of 160 $m^2\ g^{-1}$ and mesopores centered at 4.0 nm from N_2 adsorption, (ii) the crystalline walls from wide-angle XRD pattern, (iii) the wormhole-like framework from low-angle XRD pattern and TEM images, (iv) the nanobelts and nanowires morphology from TEM images, and (v) Si–O–Nb and Si–N–Nb bonds from FTIR spectroscopy.

Keywords: Niobium-silicon oxynitride; Nitridation; Characterization

1. Introduction

Niobium nitrides are well known for their refractory, electronic and magnetic properties. They have already found application in cutting tools, wear-resistant parts and hard coatings and as electronic and magnetic components and superconductors [1]. Fruitful application of niobium oxynitrides and carbides in heterogeneous catalysis is still to be achieved. There are a few reports in this area. Brayner et al. [2] prepared extruded niobium oxynitrides with meso and macropores and tested them in the cyclohexane dehydrogenation reaction. Niobium oxynitride prepared by supporting it on alumina was active in thiophene hydrodesulfurization (HDS), but it is less stable than molybdenum and tungsten oxynitrides when exposed to air [3].

Nitrides are commonly prepared by carbothermic nitridation process that starts with carbon and metal oxides reactants in a nitrogen atmosphere or via direct interaction between transition metals and dinitrogen or ammonia [4]. In the Nb–N system the following compounds exist: Nb_2N-β-phase (hexagonal), Nb_4N_3-γ-phase (tetragonal), and NbN-δ-phase (cubic) [5]. Other subnitrides, Nb_5N_2 and Nb_3N_2 clusters, can be produced in molecular beams with laser vaporization of niobium in nitrogen atmosphere at 300 K [6]. The NbN synthesis occurs at a relatively high temperature (1160 K) in a single step transformation of $Nb_2O_5 \rightarrow NbN$ via NbN_xO_{1-x} intermediates [7].

On the other hand, the structural chemistry of silicon nitride has analogues in the tetrahedral SiO_4 units in silicates. Silicon nitride forms a class of network structures with corner sharing SiN_4-tetrahedra. This allows the design of porous materials and pore size engineering similar to those in micro and mesoporous silica materials. Recently there has been considerable interest in high surface area silicon nitride for catalytic applications. Dismukes et al. [8] have reported microporous polysilazane-derived materials ($Sg > 500\ m^2\ g^{-1}$). Bradley et al. [9–11] have studied the synthesis of microporous high surface area silicon imido nitride ($Sg = 400\ m^2\ g^{-1}$) using organometallic precursors and sol–gel methods. Surface nitridation of aerosol [12,13], SBA-15 [14,15] and MCM-41 [16] affords high surface area materials (150, 1000, and 600 $m^2\ g^{-1}$, respectively) as well but complete nitridation is not achieved. Mesoporous silicon nitride materials with narrow pore size distributions were obtained from silicon halides and ammonia in organic solvents at room temperature and subsequent dehalogenation at $T > 723$ K [17].

The ammonolysis of the mixture of niobium chloride and silicon chloride has been studied in order to prepare nanoporous silicon-niobium nitride with high surface area. Various complimentary techniques were applied in order to elucidate the obtained structure, i.e., to confirm both the mesostructural ordering and pore wall crystallinity. FTIR and ^{29}Si NMR spectroscopies verified the incorporation of N into the material.

* Corresponding author. Tel.: +48 61 8291207; fax: +48 61 8658008.
E-mail address: nowakiza@amu.edu.pl (I. Nowak).

0920-5861/$ – see front matter
doi:10.1016/j.cattod.2006.07.028

To our knowledge, the direct nitridation of niobiosilica precursor by ammonia has not been reported so far.

2. Experimental

2.1. Synthesis

The synthetic strategy that we have adopted from Ref. [17] uses metal/non-metal halides as starting materials to assemble silicon-niobium nitride. All operations were performed using a glove box. In our study we have used niobium and silicon chlorides diluted with heptane as a precursor solution to obtain porous niobium-silicon nitride materials by reaction with ammonia. The solvent was dried (over molecular sieves) prior to use. Silicon chloride (Acros, 99.8%) was diluted with heptane (Fluka, spectroscopic grade, 96 cm^3) to get a 4 vol.% solution and then niobium(V) chloride (Acros, 99.8%) in the stoichiometric molar ratio of Nb:Si = 1:1 was added. The mixture was flushed at room temperature for few hours with dried gaseous ammonia to give a yellowish precipitate and ammonium chloride. The mixture was filtered and dried at 323 K for few hours. The precipitate was dechlorinated in a tube furnace. The yellowish material was placed in a boat in a horizontal quartz tube ammonia flow reactor (30 cm^3 min^{-1}), heated at a rate of 5 K min^{-1} to 873 K and annealed at that temperature for 2 h. During this process a white powder (NH_4Cl) was formed at the end-of-tube. The evolution of the ammonium chloride from the as-synthesized products to yield the oxinitride nanoparticles was achieved.

2.2. Characterization

N-containing catalyst was characterized to find:

- chemical formula by XRF, CHN analyses and TG/DTG measurement;
- mesoporous phase identification and phase purity by XRD;
- morphology and textural properties by TEM;
- crystallinity, unit cell volume and crystallographic phases by XRD;
- surface area, pore size distribution and surface properties by nitrogen sorption;
- niobium environment in the structure by H_2-TPR;
- silicon environment in the structure by ^{29}Si NMR spectroscopy;
- surface properties by FTIR spectroscopy with nitrogen(II) oxide (NO) as a probe molecule.

Si and Nb contents were determined by X-ray fluorescence (XRF) (Shimadzu EDX 700 equipment), while C, H, N by using a microanalysis with an Elementar VARIO ELIII Elemental Analyzer.

Samples for transmission electron microscopy (TEM) were prepared by the grinding of the powder and successive ultrasonic treatment in isopropyl alcohol for 1 min. A drop of the suspension was dried on the standard TEM sample grid covered with holey carbon film. JEOL 2000 electron microscope operating at 80 kV was used for observations.

The Fourier transform infrared spectra (FTIR) were recorded using a Bruker FTIR Vector 22 spectrometer working with a globar lamp source, a KBr beam splitter, and DTGS/KBr detector. In the employed system it has been possible to cover the 400–4000 cm^{-1} range. The resolution was selected to be 2 cm^{-1} and the number of scans, 128. The samples were dispersed in KBr pellet (with slight grinding) for FTIR measurements at room temperature or were pressed (under low pressure) into thin self-supporting wafers of ~10 mg cm^{-2} and placed in a conventional high-vacuum cell for the activation and adsorption (nitrogen(II) oxide) treatments. Spectra were recorded at the room temperature (RT).

The X-ray diffraction (XRD) patterns of the powder materials were recorded by a TUR-62 diffractometer using a Ni-filtered Cu Kα radiation operating at 40 kV and 30 mA. The 2Θ range started from 1.4° and with a step of 0.02°. The $h\,k\,l$ indexes of materials were calculated based on the Bragg diffraction equation.

Micromeritics 2010 was used to measure the nitrogen adsorption/desorption isotherms of the materials. Prior to the measurements, the materials were outgassed at 573 K for 3 h. The BET specific surface area was calculated using BET equation in the range of relative pressure between 0.05 and 0.25. The BJH methods was used to calculate the pore volume and the pore size distribution with the use of the desorption branch of the isotherm.

Thermal analyses – thermogravimetry, derivative thermogravimetry (TG, DTG), and differential scanning calorimetry (DSC) – were performed on a TG Setaram SetSys12 thermobalance in air or helium flow with an 11 mg sample. The heating rate was 10 K min^{-1} (temperature range: 303–1103 K).

To evaluate the reducibility of Nb species in the samples, H_2-temperature programmed reduction (H_2-TPR) was conducted, using a TPR apparatus (Micromeritics 2705). A sample (0.04 g) was pretreated in a flow of He at 723 K for 1 h and then cooled to room temperature. Lastly the reduction of the sample was carried out in a H_2/Ar (10 vol.%) flow of 40 cm^3 min^{-1} from room temperature up to 1373 K with a ramp of 10 K min^{-1}. Outlet H_2 concentration was monitored continously using a TCD, which allowed the evaluation of H_2 consumption.

^{29}Si MAS NMR experiments were carried out on a Bruker Avance 300dmx spectrometer operating at 59.62 MHz. A 10 mm MAS probe head was used with a speed of 4000 Hz. ^{29}Si spectra were recorded with cross polarization (CP) and chemical shifts are in ppm with respect to Q8M8 (δ = 12.04 ppm).

3. Results and discussion

A blackish grey solid was obtained after dechlorination. XRF analysis showed that the molar ratio of silicon to niobium in the product was 1 ± 0.001, exact as in the precursor mixture. Elemental and XRF analyses of a new material gave values of 13.5% N, 1.7% H, 47.5% Nb and 14.3% Si. From

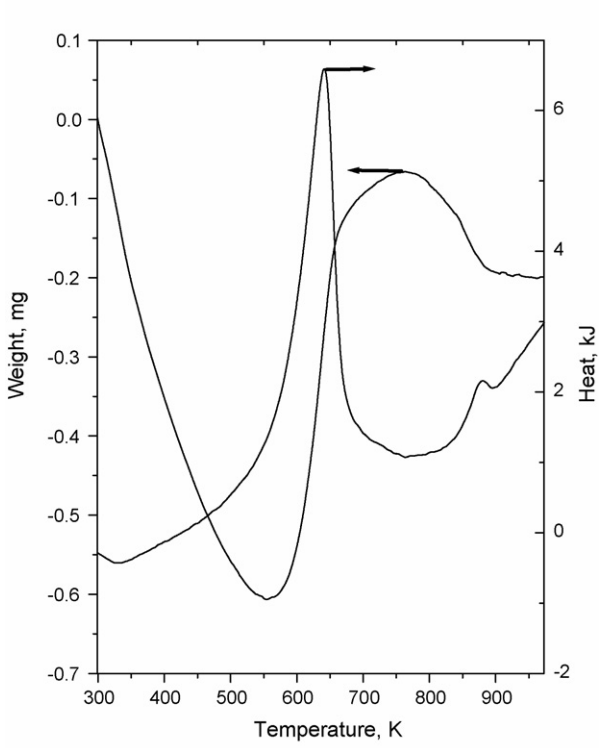

Fig. 1. TG/DSC analyses in air for NbSiNO materials.

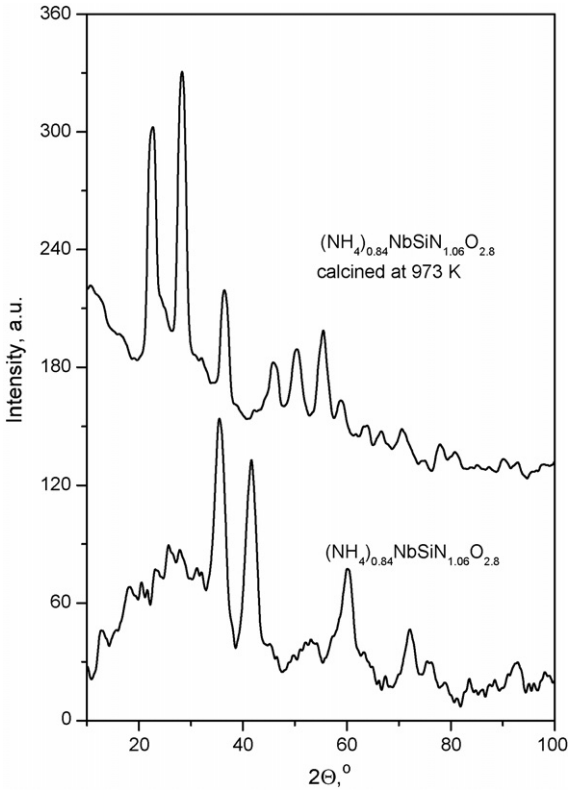

Fig. 2. X-ray diffraction patterns for NbSiNO samples.

these data and DTG measurements (the weight changes from nitride via oxinitride and oxide) a molecular formula of $(NH_4)_{0.84}NbSiN_{1.06}O_{2.8}$ can be calculated. This is an indication that the prepared ''NbSiON'' is non-stoichiometric and defective.

The TG, DTG and DSC curves provide information on the thermal stability and thermal decomposition of NbSiON. Thermogravimetric analyses (TG/DTG) performed in static air determined the oxidation onset temperature of the oxynitride. Fig. 1 presents the thermal analyses' curves. The oxidation reaction starts at ca. 300 K and continued up to 550 K (the maximum on the DTA). Moreover, TG/DTA/DSC measurements of the material revealed an increase of sample weight upon performing experiment in air until 640 K. Such peak (exothermic) was not observed in helium and comes from the exchange of nitrogen by oxygen. Oxidation into Nb_2O_5 is completed at a temperature of 750 K. The second observed peak at 873 K was attributed to the formation of crystalline orthorhombic niobia. The latter feature can be elaborated on the basis of an exothermic peak registered without mass loss, indicating a phase transition, assigned to crystallization of Nb_2O_5 [18]. From the above results, it is clear that most of the nitrogen in the as-synthesized powder is completely eliminated and that only $Nb_2O_5{\cdot}2SiO_2$ is present. Little further weight loss in the TG curve is observed at temperature above 973 K (not shown in Fig. 1), indicating the completion of any reaction involving a weight change.

Wide-angle XRD patterns of as made $(NH_4)_{0.84}NbSiN_{1.06}O_{2.8}$ and the sample calcined at 973 K for 2 h are shown in Fig. 2. These patterns reveal a new crystal structure that can be indexed in *Pm3m* space group. The a_0 cell-parameter value for the N-containing sample was calculated using the cubic indexing method. The XRD pattern can be indexed to the (0 0 1), (1 1 0), (1 1 1), (2 1 1), (2 2 0), (3 0 0), (3 1 0), (3 1 1), and (3 2 0) diffraction planes of $(NH_4)_{0.84}NbSiN_{1.06}O_{2.8}$ (not calcined). The a_0 cell parameter value for the NbSiON sample was 0.370 nm which was smaller than the value for calcined at 973 K sample (0.554 nm). It indicates that niobium could enter the silica lattice, resulting in the formation of mixed oxides. Traces of Si_3N_4 phases (upon high magnification) were observed. XRD analysis of calcined sample shows that sintering at 973 K for 2 h in an air is enough to transform oxynitride to oxide as only Nb_2O_5 phase (orthorhombic; JCPDS file 27-1003) was present. One major peak in the low-angle range (not shown here) at around $2\Theta = 1.92^\circ$ [denoted as (1 0 0)] was observed. The intensity of the d_{100} peak was relatively weak. This peak proves the existence of a mesoporous structure, but the pores are irregular in shape (e.g., wormhole-like).

The nitrogen adsorption isotherm for $(NH_4)_{0.84}NbSiN_{1.06}O_{2.8}$ (Fig. 3A) at 77 K displays an inflection in the relative pressure (p/p_0) range of 0.4–0.9, indicating the characterization of capillary condensation within mesopores. The hysteresis is characterized by a sharp step in the desorption isotherm that has previously been ascribed to delayed capillary evaporation from (meso)pores with narrow constrictions. Moreover, the broad hysteresis loop in the isotherm demonstrates the disorder in the shape of some mesopores, which limits the emptying and filling of the accessible volume. This is consistent with the results of the XRD measurements. The relative adsorption isotherm shown in Fig. 3A was used for α_s

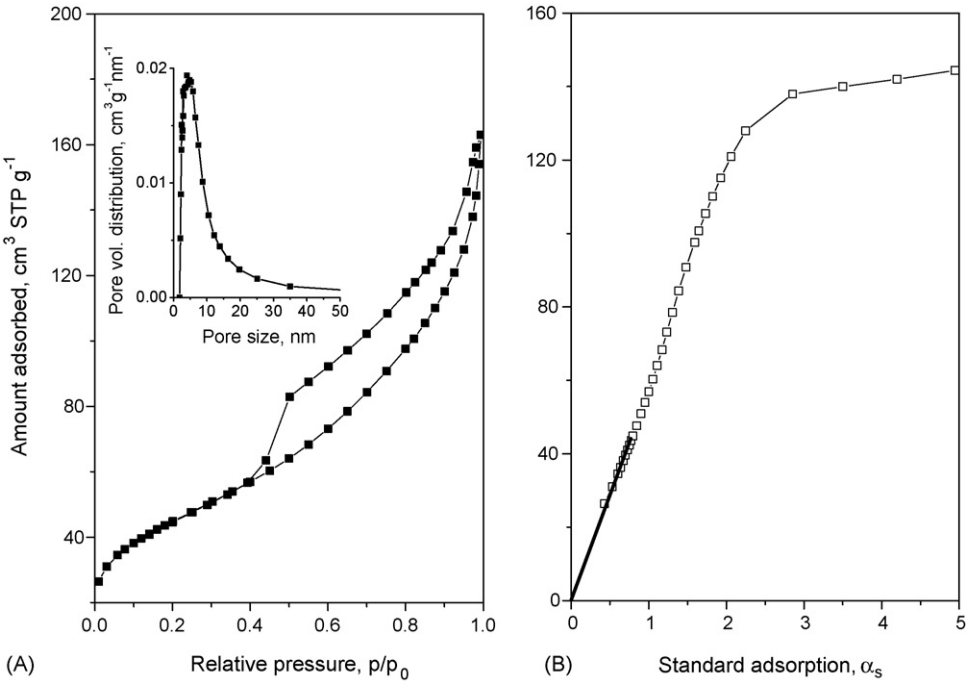

Fig. 3. Nitrogen adsorption/desorption data at 77 K for $(NH_4)_{0.84}NbSiN_{1.06}O_{2.8}$ (not calcined). (A) Isotherm and pore size distribution (onset). (B) α_s-plot.

plot analysis (Fig. 3B) that confirms mesoporosity of the $(NH_4)_{0.84}NbSiN_{1.06}O_{2.8}$ material. Such α_s plots demonstrated upward deviations in the region beyond the standard adsorption of ~1.2 indicate capillary condensation in mesopores and a gradual inflection up to $\alpha_s = 3$ which suggests a broader pore size distribution. The pore size distribution (Fig. 3A onset) is centered at 4.0 nm and is rather broad. BET surface area of 160 $m^2\ g^{-1}$ suggests a potentially useful mesoporous material.

The XRD and nitrogen adsorption results were verified by transmission electron microscopy. The presence of a disordered wormhole-like mesostructure is apparent (Fig. 4, left). The observed disorder is consistent with the XRD, which shows the absence of additional indexable peaks in the pattern besides the broad low-angle d_{100} peak. Moreover, it is seen that the product is a mixture of nanotubes (diameter of 25–30 nm and length up to 300 nm) and nanoparticles (Fig. 4, right). For the pore topology, there is no long-range order in the pore structure from Fig. 4. However, the sample has clearly mesostructure and displays the pattern characteristic of the pore-packing motif that can be described as having wormhole-like topology. Similar patterns can be observed in some works [19]. The wormhole-like framework mesostructure is a potentially important structural feature and will have a prospective application for catalytic reactivity, in part, because channel branching within the framework can facilitate access to reactive sites on the framework wall.

The H_2-TPR profiles for $(NH_4)_{0.84}NbSiN_{1.06}O_{2.8}$ and the sample oxidized in air at 973 K are illustrated in Fig. 5.

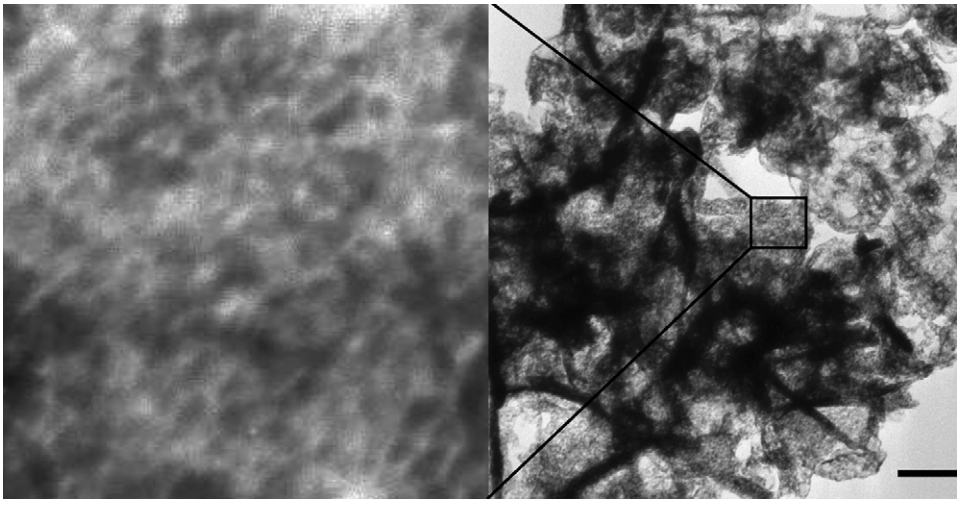

Fig. 4. Transmission electron microscopy images for $(NH_4)_{0.84}NbSiN_{1.06}O_{2.8}$ (not calcined). The marker represents 100 nm.

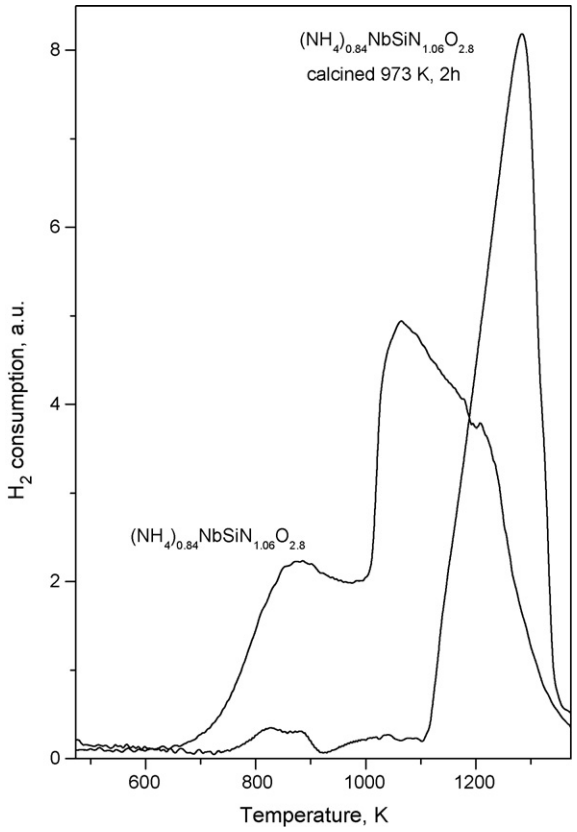

Fig. 5. H_2-temperature programmed reduction profiles for NbSiNO samples.

The TCD signals correspond primarily to H_2 consumption and the production of H_2O. Reduction of these catalysts occurred in the temperature range of 623–1373 K. It is well known [20], that a reduction of Nb^{+5} in Nb_2O_5 yields an intense maximum at 1173 K. H_2-TPR revealed that in N-containing sample (Fig. 5) niobium is present in at least three different forms and states: a low temperature peak at around 873 K, an intermediate temperature peak at ~1050 K and third high temperature peak at around 1175 K. From the above finding the lower oxidation state can be postulated, i.e. ~+4 basing on the following consideration. After calcination H_2 consumption at low temperature decreased markedly, while at high temperatures it increased and thus it can be concluded that the oxidation state is increased leading to the profile similar to that one observed for nanoniobia. The oxidation of the niobium oxynitrides implies the oxygen/nitrogen substitution and the transformation of the reduced valency state of niobium (probably $Nb^{\pm 4.0}$) into Nb^{+5}. The weight gain measurements confirm the nitrogen content given by CHN measurements and are consistent with the calculated niobium valency of the NbSiON.

The N-containing sample displays several FTIR absorbance bands (Fig. 6): at 3159 cm^{-1}, which is attributed to the stretching NH bands ν (N–H) and bands at 1401 and 1632 cm^{-1} that can be assigned to δ_{as} (NH_4^+) of NH bonded to a Si–OH hydroxyl group and the presence of adsorbed NH_3 or/and water. The shift from 1100 cm^{-1} – typical of silica – to 1070 cm^{-1} and a presence of a band Si_2N vibration is observed upon incorporation of nitrogen. The N-containing material is perceptibly free from amorphous silica impurities, as evidenced by the poorly resolved bands (at 1254–1220 and

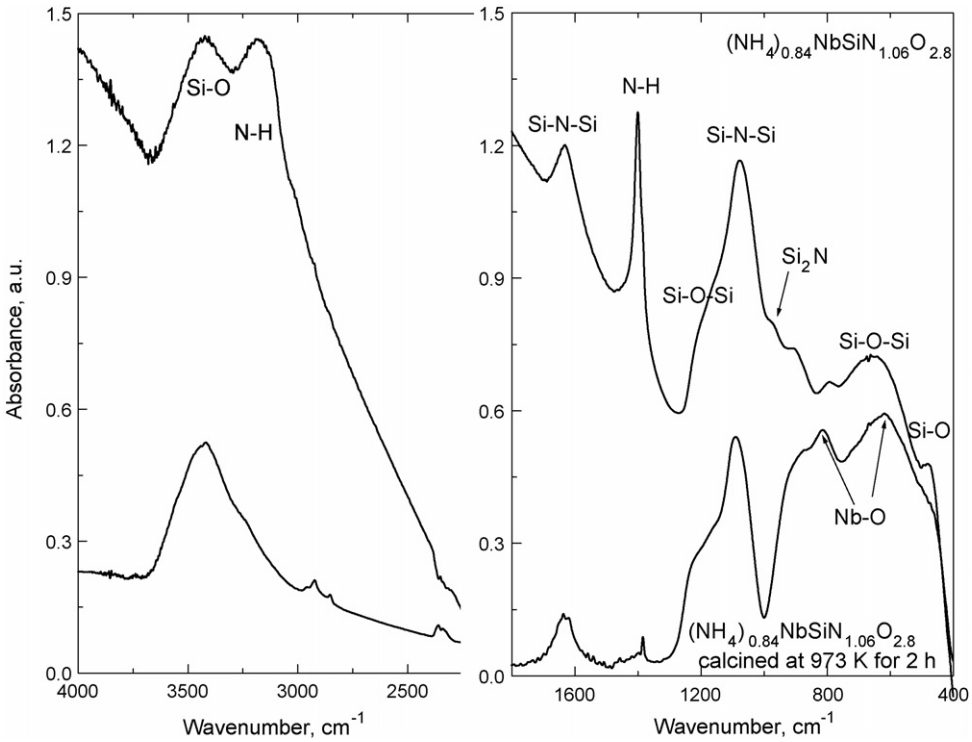

Fig. 6. FTIR spectra of $(NH_4)_{0.84}NbSiN_{1.06}O_{2.8}$ samples in KBr matrix.

796–784 cm^{-1}). The FTIR spectra did show neither silanol (Si–OH; 3750 cm^{-1}) or hydroxyl (Nb–OH; 3600 cm^{-1}) nor silazane bands ($SiNH_2$; 3359 cm^{-1}). The spectrum, however does show an intense band at ca. 1430 cm^{-1} that has decreased after the activation in vacuum has been applied.

The surface properties of the N-containing sample were studied by NO interaction with the niobium-species by analysis of the in situ FTIR spectra in the 1300–2200 cm^{-1} region. The adsorption of NO at RT did not lead to the formation of nitrato/nitrito species at the wavenumbers below 1600 cm^{-1}, thus the sample do not have oxidizing properties observed for niobiosilica of MCM-41 type (NbMCM-41) [21]. This feature was further proved via zero activity in cyclohexene epoxidation reaction done at 318 K in acetonitrile using hydrogen peroxide as oxidant.

Very weak signals in the ^{29}Si NMR spectra were obtained from $(NH_4)_{0.84}NbSiN_{1.06}O_{2.8}$ and $(NH_4)_{0.84}NbSiN_{1.06}O_{2.8}$ calcined in air at 973 K. This indicates the absence of hydrogen, which confirms the in situ FTIR conclusions and originates from ill defined local structure. However, some trend can be observed. The ^{29}Si NMR spectra of $(NH_4)_{0.84}NbSiN_{1.06}O_{2.8}$ showed a broad peak in the range (−65 to −117 ppm). There can be many species assigned in this region starting from SiN_3O (−63 ppm), SiN_2O_2 (−78 ppm), up to $SiNO_3$ (−90 ppm) and SiO_4 (−110 ppm) [22,23]. This indicates that the pure niobium silicon nitride and silica phases diffuse into each other, leading to the formation of a mixed niobium silicon oxynitride. The maximum of the main broad line shifts from −94 ppm for $(NH_4)_{0.84}NbSiN_{1.06}O_{2.8}$ to −104 ppm for N-containing sample calcined at 973 K, thus for niobia–silica sample. The NMR spectrum analysis confirmed the formation of different Si–N–O or Si–O–N bonding ($NbSiN_xO_y$).

4. Conclusions

In this work we presented our new finding from experiments directed toward an easy way to establish a new composition of Si–Nb–O–N. Our synthetic concept used chlorides of niobium and silicon as molecular precursors.

In summary, a mesoporous niobium-silicon oxynitride with high surface area, wide pore size distribution in the mesopore range, crystallinity and catalytic properties has been prepared. It seems that the oxynitride anions form polymeric structures with bridging nitride/oxide groups such like $[NbSiO_yN_z]^{-x}$ cages clustered in the manner of the $(AlSiO_4)^-$ units of sodalite. Powder XRD patterns, TEM images and nitrogen adsorption–desorption isotherm measurements have verified the formation of NbSiNO nanoparticles. The N-doped niobiosilica materials exhibit both mesoporosity and high level of crystalloid character.

Acknowledgement

The authors thank the Polish Ministry of Scientific Research and Information Technology (grant No 3T09A 10026; 2004–2007) for the financial support.

References

[1] I. Nowak, M. Ziolek, Chem. Rev. 99 (1999) 3603.
[2] R. Brayner, J.A.J. Rodrigues, G.M. Cruz, Catal. Today 57 (2000) 219.
[3] R. Brayner, G. Djéga-Mariadassou, G.M. Cruz, J.A.J. Rodrigues, Catal. Today 57 (2000) 225.
[4] R. Niewa, H. Jacobs, Chem. Rev. 96 (1996) 2053.
[5] A.G. Aleksanyan, S.K. Dolukhanyan, Int. J. Hydrogen Energy 26 (2001) 429.
[6] D.-S. Yang, P.A. Hackett, J. Electron Spectrosc. Related Phenom. 106 (2000) 153.
[7] R. Kapoor, S.T. Oyama, in: M.A. Serio, et al. (Eds.), Synthesis and Characterization of Advanced Materials, American Chemical Society, Washington, 1998, p. 211.
[8] J.P. Dismukes, J.W. Johnson, J.S. Bradley, J.M. Millar, Chem. Mater. 9 (1997) 699.
[9] O. Vollmer, F. Lefebvre, J.S. Bradley, J. Mol. Catal. A: Chem. 146 (1999) 87.
[10] R. Rovai, C.W. Lehmann, J.S. Bradley, Angew. Chem. Int. Ed. 38 (1999) 2036.
[11] J.S. Bradley, O. Vollmer, R. Rovai, U. Specht, F. Lefebvre, Adv. Mater. 10 (1998) 938.
[12] P.W. Lednor, R. de Ruiter, J. Chem. Soc., Chem. Commun. (1991) 1625.
[13] R.W. Chorley, P.W. Lednor, Adv. Mater. 3 (1991) 474.
[14] N. Chino, T. Okubo, Micropor. Mesopor. Mater. 87 (2005) 15.
[15] J. Wang, Q. Liu, Micropor. Mesopor. Mater. 83 (2005) 225.
[16] J. El Haskouri, S. Cabrera, F. Sapina, J. Latorre, C. Guillem, A. Beltran-Porter, D. Beltran-Porter, M.D. Marcos, P. Amoros, Adv. Mater. 13 (2001) 192.
[17] S. Kaskel, D. Farrusseng, K. Schlichte, J. Chem. Soc., Chem. Commun. (2000) 2481.
[18] T. Ushikubo, Catal. Today 57 (2000) 331.
[19] Y.Q. Wang, X.H. Tang, L.X. Yin, W.P. Huang, Y.R. Hacohen, Adv. Mater. 12 (2000) 1183.
[20] F.M.T. Mendes, C.A. Perez, R.R. Soares, F.B. Noronha, M. Schmal, Catal. Today 78 (2003) 449.
[21] M. Ziolek, I. Sobczak, A. Lewandowska, I. Nowak, P. Decyk, M. Renn, B. Jankowska, Catal. Today 70 (2001) 169.
[22] K. Wan, Q. Liu, C. Zhang, J. Wang, Bull. Chem. Soc. Jpn. 77 (2004) 1409.
[23] R.S. Aujla, G. Leng-Ward, M.H. Lewis, E.F. Seymour, G.A. Steyles, G.W. West, Phil. Mag. B 54 (1986) L51.